

RESEARCH

Open Access



Double-negative T cells in combination with ursodeoxycholic acid ameliorates immune-mediated cholangitis in mice

Chunpan Zhang^{1,2,3†}, Guangyong Sun^{4,5,6†}, Hua Jin^{4,5,6}, Yunxiong Wei^{4,5}, Shimeng Zheng^{4,5}, Xiyu Wang^{4,5}, Xinyan Zhao^{1,2,3}, Dong Zhang^{4,5,6,7*} and Jidong Jia^{1,2,3*}

Abstract

Background Primary biliary cholangitis (PBC) is a liver-specific autoimmune disease. Treatment of PBC with ursodeoxycholic acid (UDCA) is not sufficient to prevent disease progression. Our previous study revealed that the number of hepatic double-negative T cells (DNT), which are unique regulatory T cells, was reduced in PBC patients. However, whether replenishment of DNT can prevent the progression of PBC remains unclear.

Methods DnTGFβRII (Tg) mice and 2OA-BSA-immunized mice received DNT alone or in combination with oral UDCA. After 6-12 weeks of treatment, these mice were assessed for serological changes, liver pathological manifestations and intrahepatic immune responses.

Results Adoptive transfer of DNT alone significantly decreased serum levels of alanine transaminase (ALT), aspartate transaminase (AST), antimicrobial antibody M2 (AMA-M2) and immunoglobulin M (IgM) in both Tg and 2OA-BSA-immunized PBC mouse models. In addition, DNT exhibited a strong killing effect on liver T cells and strong inhibition of their proliferation, but did not significantly improve the histology of PBC liver. However, combination therapy with DNT and oral UDCA predominantly ameliorated liver inflammation and significantly inhibited hepatic T and B cells. In vitro further study revealed that UDCA up-regulated the proliferation of DNT, increased the expression of the functional molecule perforin, and reduced the expression of NKG2A and endothelial cell protein C receptor (EPCR) through the farnesoid X receptor (FXR)/JNK signaling pathway in both mice and human DNT.

Conclusions A single transfer of DNT ameliorated PBC in mice, while combination therapy of DNT with oral UDCA displayed a better efficacy, with stronger inhibition of hepatic T and B cells. This study highlights the potential application of DNT-based combination therapy for PBC, especially for UDCA non-responders.

Keywords Primary biliary cholangitis, Double-negative T cells, Ursodeoxycholic acid, Farnesoid X receptor

[†]Chunpan Zhang and Guangyong Sun contributed equally to this work.

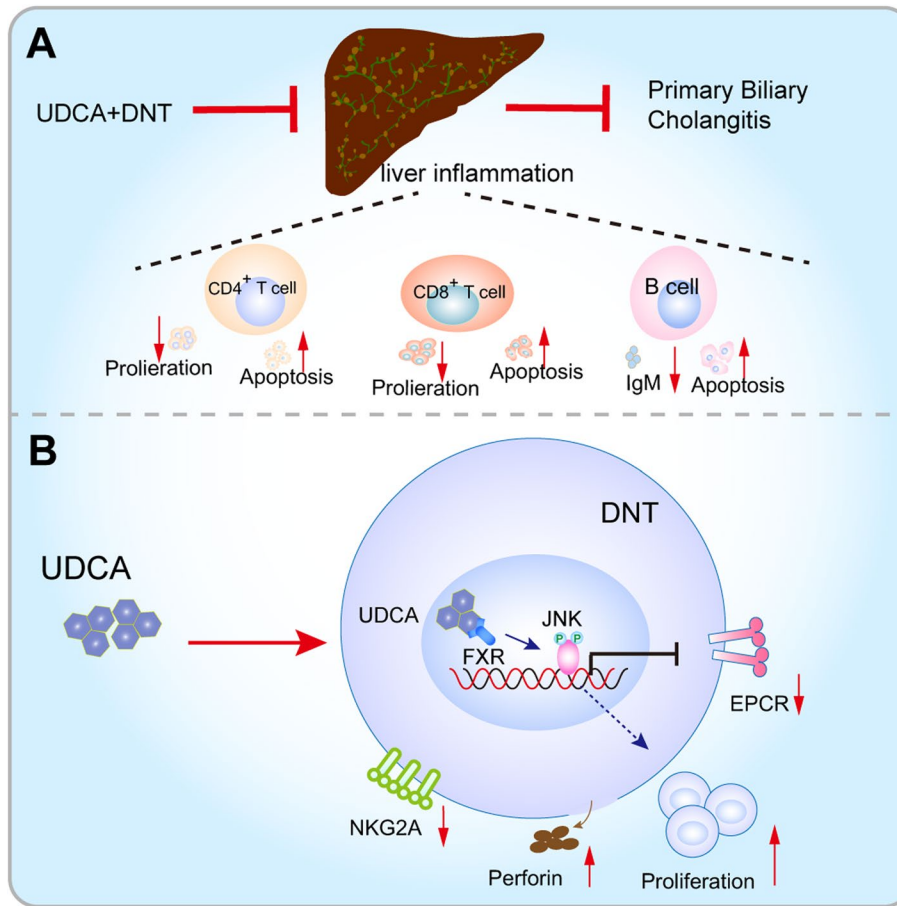
*Correspondence:

Dong Zhang
zhangd@ccmu.edu.cn
Jidong Jia
jia_jd@ccmu.edu.cn

Full list of author information is available at the end of the article



Graphical Abstract

**Background**

Primary biliary cholangitis (PBC) is a cholestatic liver disease characterized by the presence of anti-mitochondrial antibodies (AMAs) in the serum and chronic non-suppurative destructive cholangitis that affects mainly the interlobular bile ducts. If left untreated, PBC ultimately progresses to liver cirrhosis and related complications [1]. Ursodeoxycholic acid (UDCA) is the current standard of care, but it is not always sufficient to prevent disease progression. Indeed, approximately 40% of patients respond poorly to UDCA and rapidly progress to end-stage liver disease [2, 3]. Adding or switching to obeticholic acid (OCA), fibrates, or even budesonide may lead to additional biochemical improvements in some patients. However, it is important to note that these options may not be well tolerated due to significant pruritus and are contraindicated in patients with advanced cirrhosis [2, 3]. Therefore, novel therapies for PBC are highly needed.

TCR $\alpha\beta$ ⁺ double-negative T cells (DNT) are a subset of T cells with regulatory functions that do not express CD4, CD8, or NK cell surface markers, but are defined by T-cell receptor (TCR) $\alpha\beta$ ⁺ CD3⁺CD4⁻CD8⁻CD56⁻ (human) / NK1.1⁻ (mice) [4]. They are a unique type of regulatory T cells that do not express FoxP3 [5]. Currently, unlike CD4⁺CD25⁺Foxp3⁺ Treg cells, there are no unique markers for the identification of DNT. CD4⁺CD25⁺Foxp3⁺ Tregs regulate immune responses through the secretion of inhibitory cytokines such as IL-10 and TGF β , whereas DNT primarily rely on perforin and granzyme B [6, 7]. We previously demonstrated that DNT can inhibit CD11c⁺ dendritic cell function and mediate an antigen-specific protective role via the Lag3 molecule in allergic asthma [8]. Additionally, we reported that DNT prevent the development of nonalcoholic steatohepatitis (NASH) by the selective inhibition of intrahepatic Th17 cells and M1 macrophages [9].

Our previous research demonstrated a significant reduction in both the absolute number and proportion of hepatic DNT in PBC patients [10]. Moreover, DNT from PBC patients exhibited diminished immunosuppressive capacity against autologous pro-inflammatory CD4⁺ and CD8⁺ T cells compared to DNT from healthy individuals. Importantly, the frequency of these DNT was inversely correlated with disease severity. In patients treated with UDCA, we observed a significant increase in the proportion of DNT in responders compared to non-responders. These findings raised the critical question of whether replenishing DNT could represent a therapeutic strategy to prevent or ameliorate PBC progression.

Therefore, in the present study, we explored the therapeutic role of the adoptive transfer of DNT in dnTGFβRII mice and 2OA-BSA-induced PBC mice and then examined the changes in the immunological microenvironment of the liver. Furthermore, we explored combination therapy with DNT and UDCA to verify their potential therapeutic effects in PBC mouse models.

Methods

Animal models of PBC

dnTGFβRII mice (B6. Cg-Tg(Cd4-TGFBR2)16Flv/J, Strain#: 005551) were purchased from The Jackson Laboratory (Bar Harbor, Maine, USA). C57BL/6 wild-type (WT) and C57BL/6-CD45.1 (CD45.1) mice were purchased from Beijing Vital River Laboratory (Beijing, China). C57BL/6JSmoc-Nr1h4^{em1Smoc} (*Fxr*^{-/-}, Strain#: NM-KO-190328) mice were purchased from Shanghai Model Organisms (Shanghai, China). Male dnTGFβRII mice were bred with female congenic C57BL/6 mice at the animal facilities of Beijing Friendship Hospital (Beijing, China). Four-week-old mice were genotyped by polymerase chain reaction (PCR). These mice were housed in a specific pathogen-free environment with temperature control and free access to food and water. Female, age-matched (6–30 weeks old) littermate dnTGFβRII mice were used in this study. The ARRIVE guidelines were followed (Additional file 1).

2OA coupled with BSA (2OA-BSA, Cat#: 4610039-02) was purchased from Beijing Hapten and Protein Biomedical Institute. In accordance with previous methods, 100 μg of the 2OA-BSA conjugate dissolved in 50 μl of PBS (Cat#: D3922, Invitrogen, USA) was emulsified with 50 μl of complete Freund's adjuvant (CFA, containing 1 mg/mL *Mycobacterium tuberculosis* strain H37RA, Cat#: F5881, Sigma-Aldrich, USA). The emulsion was subsequently injected intraperitoneally (I.P.) into 6–8-week-old female C57BL/6 mice, and 100 ng of pertussis toxin (Cat#: 180, List Biological Laboratories, Campbell, CA) dissolved in 100 μl of PBS was also injected I.P. into these mice. Two days later, these mice were injected I.P. with 100 ng of

pertussis toxin for a second time. After 2 weeks, these mice were re-immunized with 100 μg of 2OA-BSA in 50 μl of PBS emulsified with 50 μl of incomplete Freund's adjuvant (IFA, Cat#: F5506, Sigma-Aldrich, USA) administered intraperitoneally.

Treatment protocols

The generation of DNT *ex vivo* was performed as previously described [5]. Briefly, mature dendritic cells (mDCs) were obtained from lipopolysaccharide (Cat#: L2880, Sigma-Aldrich, USA)-stimulated bone marrow cells of C57BL/6J mice and isolated using CD86-positive (Cat#: 105008, Biolegend, USA) magnetic bead separation (Cat#: 130-048-801, Miltenyi Biotec, Germany). CD4⁺CD25⁻ T cells were isolated from the spleen and lymph nodes of female WT, CD45.1, or *Fxr*^{-/-} mice and purified through T-cell enrichment (Cat#: MTCC-25, BD Biosciences, USA), followed by magnetic bead-based Ter119/TCRγδ/CD11b/NK1.1/CD8/CD25/B220-negative separation (Cat#: 130-048-801, Miltenyi Biotec, Germany). Then, these purified CD4⁺ T cells were cocultured with the above mDCs for 7 days, supplemented with 50 ng/ml rmIL-2 (Cat#: 212-12-1MG, PeproTech, USA). Finally, CD3⁺NK1.1⁻TCRβ⁺CD4⁻CD8⁻ cells were harvested from the mixed cells described above using a FACS Aria II sorter (Cat#: 643177, BD Biosciences, USA).

dnTGFβRII (Tg) mice were randomly divided into the following groups using a random number table: an untreated group (Tg); a single DNT treatment group (Tg+DNT), which received a single adoptive transfer of 2–3 × 10⁶ DNT (purity > 97%) via tail vein injection; a UDCA treatment group (Tg+UDCA), which received 15 mg/kg/day of UDCA (Cat#: U5127, Sigma-Aldrich, USA) administered intragastrically following the methods of a previous study [11]; and a combination therapy group (Tg+DNT+UDCA), which received both DNT and UDCA treatments. Similarly, 2OA-BSA-immunized mice (6 weeks after the 2nd 2OA-BSA injection) were also randomly divided into the following groups: an untreated group (Untreated); a single DNT treatment group (DNT), which received a single adoptive transfer of 2–3 × 10⁶ DNT (purity > 97%) via tail vein injection (DNT); a UDCA treatment group, which received 15 mg/kg/day of UDCA administered intragastrically (UDCA); and combination therapy groups (DNT+UDCA), which received both DNT and UDCA treatments. The corresponding author remained aware of the group allocations at all stages of the experiment. All of the mice were sacrificed at either 6–12 weeks posttreatment, and plasma, liver and colon tissue were harvested. Paraffin-embedded sections of liver and colon tissue were prepared for hematoxylin and eosin (H&E) and Sirius red staining. The severity of liver inflammation, bile duct damage,

and colitis was evaluated histologically as previously described [12–14]. Hepatic nonparenchymal cell infiltration was quantified by flow cytometry, as described in the following section. Plasma levels of alanine transaminase (ALT), aspartate transaminase (AST), anti-mitochondrial antibody M2 (AMA-M2), immunoglobulin M (IgM), and alkaline phosphatase (ALP) were measured according to the manufacturer's instructions.

DNT functional assays

CD45.1-positive B cells were isolated from the spleens of CD45.1 mice using magnetic bead-based CD19-positive separation (Cat#: 152408, Biolegend, USA). T cells isolated from the spleens of CD45.1 mice were purified through T-cell enrichment (Cat#: MTCC-25, BD Biosciences, USA). Then, DNT were incubated with these CD19⁺ B cells and anti-mouse CD40 (5 µg/ml, Cat#: 102811, Biolegend, USA) or cocultured with these isolated T cells and mDCs for 5 days. The apoptosis of B cells or CD4⁺ and CD8⁺ T cells was determined via Annexin V (Cat#: 640945, BioLegend, USA) staining on the 3rd day. The proliferation of CD4⁺ and CD8⁺ T cells was detected via a 5-(and 6)-carboxyfluorescein diacetate succinimidyl ester kit (CFSE, Cat#: 423801, Biolegend, USA) on the 5th day. The level of IgM produced by CD45.1-positive B cells in the culture supernatants was measured using an enzyme-linked immunosorbent assay kit (Cat#: CME0060, 4A Biotech, China) according to the manufacturer's instructions.

To verify the role of FXR on DNT, DNT (either WT or *Fxr*^{-/-}) were pretreated with dimethyl sulfoxide (DMSO, 60 µM, as a control), UDCA (60 µM), OCA (0.5 µM), z-guggulsterone (GGs, 5 µM), a combination of UDCA (60 µM) and OCA (0.5 µM), or a combination of GGs (5 µM) and UDCA (60 µM) for 48 h. These cells were subsequently cocultured with CD45.1-positive T cells or B cells for an additional 3 days. Afterward, the apoptosis of CD4⁺ T cells, CD8⁺ T cells, and B cells was detected via flow cytometry.

EdU staining protocol

Purified DNT (2×10^5 cells/well) were cultured in 96-well flat-bottom plates pre-coated with 5 µg/mL anti-mouse CD3 antibody (Biolegend, USA). Cells were maintained in 200 µL of complete medium (CM) supplemented with 2 µg/mL anti-mouse CD28 antibody (Biolegend, USA) and either DMSO (vehicle control), UDCA, OCA, GGs, withaferin A (WA), or JNK inhibitor XVI (JNK-IN8). After 48 h of incubation, and 12 h before harvest, 5-ethynyl-2'-deoxyuridine (EdU) was added to the cultures (final concentration of 50 µM). Subsequently, cells were harvested and fixed with 4% formaldehyde (100

µL/well) for 15 min at room temperature (RT), followed by two washes. Cells were then permeabilized with 0.1% Triton X-100 (100 µL/well) for 15 min at RT and washed twice. The EdU click reaction was performed by incubating the cells with 200 µL of staining solution (Cat#: C10310-2, RiboBio, China) for 30 min at RT in the dark. Finally, cells were washed and resuspended in PBS for analysis.

Flow cytometry analysis

The cells were harvested, and the expression of various cell surface markers was analyzed by flow cytometry. All surface markers were directly stained for 20–30 min at 4 °C. For intracellular staining, the cells were first fixed with Intracellular Fixation Buffer (Cat#: 420801, Biolegend, USA) for 40 min at 4 °C. Next, the cells were permeabilized with Permeabilization Buffer (Cat#: 421002, Biolegend, USA). Finally, the cells were stained with specifically against granzyme B (Cat#: 372208, Biolegend, USA), perforin (Cat#: 308106, Biolegend, USA), and phosphor c-Jun N-terminal kinase (p-JNK, Cat#: ab124956, Abcam, USA) for a minimum of 40 min at 4 °C. The secondary antibody used was goat anti-rabbit IgG (Cat#: ab150077, Abcam, USA), incubated with the samples for 30 min at 4 °C.

For nuclear staining, the cells were fixed and permeabilized using a Transcription Factor Staining kit (Cat#: 00-5523-00, Invitrogen™, USA). Subsequently, nuclear antibodies, the cells were stained with nuclear antibodies, including anti-FXR (Cat#: ab129089, Abcam, USA) and anti-Ki67 (Cat#: 652406, Biolegend, USA), for at least 40 min at 4 °C. Rabbit monoclonal IgG (Cat#: ab172730, Abcam, USA) was used as an isotype control for p-JNK and FXR. All samples were acquired on an Aria II flow cytometer (BD Biosciences), and the data were analyzed using FlowJo software v10 (Treestar, USA).

Liver histological examination

The severity of liver inflammation and bile duct damage was evaluated by one pathologist in a blinded manner as previously described [12, 13]. The degree of portal inflammation was scored based on the most severe lesions as follows: 0, no change; 1, minimal inflammation; 2, mild inflammation; 3, moderate inflammation; and 4, severe inflammation. In addition, the bile duct damage score was evaluated for the most severe lesions as follows: 0, no change; 1, epithelial damage (only cytoplasmic changes); 2, epithelial damage with cytoplasmic and nuclear changes; 3, nonsuppurative destructive cholangitis; and 4, bile duct loss.

The positive area of Sirius red staining was calculated using ImageJ software (NIH, USA).

Real-time PCR

Total RNA was extracted from the liver tissue and cells using TRIzol reagent (Cat#: T9424, Sigma-Aldrich, USA) in accordance with the manufacturer's protocol and reverse transcribed to cDNA using a Prime Script[®] RT reagent kit (Cat#: RR036A, Takara, Japan). Quantitative real-time PCR analysis was performed using an ABI 7500 Sequence Detection System (Applied Biosystems, USA) and SYBR Green Master Mix (Cat#: A25742, Applied Biosystems, CA, USA) in accordance with the manufacturer's instructions. Gene expression was normalized against the expression of the housekeeping gene *Gapdh*. The sequences of the primers used in this study are listed in Additional file 2: Table S1.

Transcriptome sequencing and biological function analysis

WT and *Fxr*^{-/-} DNT were stimulated with anti-mouse CD3 (Cat#: 100256, Biolegend, USA) and anti-mouse CD28 (Cat#: 117003, Biolegend, USA) antibodies, with or without UDCA (60 μM), for 48 h. Total RNA was subsequently extracted using TRIzol reagent. Transcriptome sequencing libraries were generated using the NEBNext[®] Ultra[™] RNA Library Prep Kit for Illumina[®] (NEB, USA) according to the manufacturer's recommendations and sequenced using an Illumina HiSeq platform (Illumina, CA).

All data and materials supporting the findings of this manuscript are presented in the paper and/or the supplemental information. The mRNA sequencing data reported in this work have been uploaded to the National Center for Biotechnology Information (NCBI) Gene Expression Omnibus (GEO) database under accession numbers GSE167116 (<https://www.ncbi.nlm.nih.gov/geo/query/acc.cgi?acc=GSE167116>) and GSE215278 (<https://www.ncbi.nlm.nih.gov/geo/query/acc.cgi?acc=GSE215278>). The analyzed data sets generated during the study are available from the corresponding author on reasonable request.

Human DNT study

Peripheral blood was obtained from healthy volunteers, and DNT were enriched using the Double-negative T-Cell Isolation Kit (Cat#: 130-092-614, Miltenyi Biotec, Germany). Then, these cells were cultured in X-vivo medium supplemented with an anti-human CD3 antibody (2 μg/mL, Cat#: 317348, BioLegend, USA) and 50 ng/mL recombinant human interleukin 2 (rhIL-2, Cat#: 200-02, Peprotech, China). On day 21, the cells were harvested and counted, and their viability, composition, and purity were assessed via flow cytometry (purity > 95%). These DNT were subsequently cultured with DMSO or UDCA for 48 h.

Statistical analysis

Statistical analyses were performed using GraphPad Prism software (version 9.0, San Diego, California, USA). Initially, all experimental data were tested using the Shapiro–Wilk test to assess normality. The values are presented as the mean ± SD for normally distributed data, while the median and IQR are used to represent nonnormally distributed data. Differences between two groups were evaluated using Student's t test for normally distributed variables and the Mann-Whitney U test for nonnormally distributed variables. Multiple comparisons were analyzed using one-way ANOVA followed by Bonferroni post hoc test for normally distributed variables and the Kruskal-Wallis test for nonnormally distributed variables (SPSS 23). Based on preliminary experiments, for the in vivo experiment, a sample size of $n=6$ per group was determined to be sufficient to detect an effect size of 0.775 with a significance level (α) of 0.05 and a statistical power of 0.8 ($1-\beta$). The total number of mice used was 24 and there were no exclusions in each experiment. While for the in vitro experiment, each group comprises 4–6 samples. Furthermore, to ensure reliability, all experiments were repeated 2–3 times. For all analyses, a value of $P \leq 0.05$ was considered to indicate a significant difference; * $P \leq 0.05$; ** $P \leq 0.01$; NS, indicates no significance.

Results

Adoptive transfer of DNT, especially DNT combined with oral UDCA, improved pathological changes in PBC mice

As shown in Fig. 1A, adoptively transferred CD45.1⁺ DNT primarily localized to the liver and draining lymph nodes, with minimal presence in the spleen or inguinal lymph nodes. Following 6–8 weeks of treatment, both the proportion of total DNT within the CD3⁺ population and the proportion of CD45.1⁺ DNT increased significantly in the liver (Fig. 1B). The absolute number of adoptively transferred DNT also increased significantly in the liver (Fig. 1B). *Cxcl9*, *Cxcl10* and *Cxcl11* were significantly upregulated in the livers of dnTGFβRII mice (Fig. 1C). Compared with untreated mice, ALT and AST levels were significantly reduced in mice treated with DNT alone (Fig. 1D). Similarly, DNT treatment significantly decreased the levels of AMA-M2 and IgM (Fig. 1E). Additionally, DNT combined with UDCA further decreased the levels of ALT, AST, AMA-M2 and IgM (Fig. 1D, E).

In contrast, neither DNT therapy alone nor UDCA treatment alone significantly improved the liver histology of PBC mice, whereas DNT therapy combined with UDCA significantly improved portal inflammation ($p=0.015$) and bile duct damage ($p=0.002$, Fig. 1F, G). Compared with DNT therapy alone and UDCA

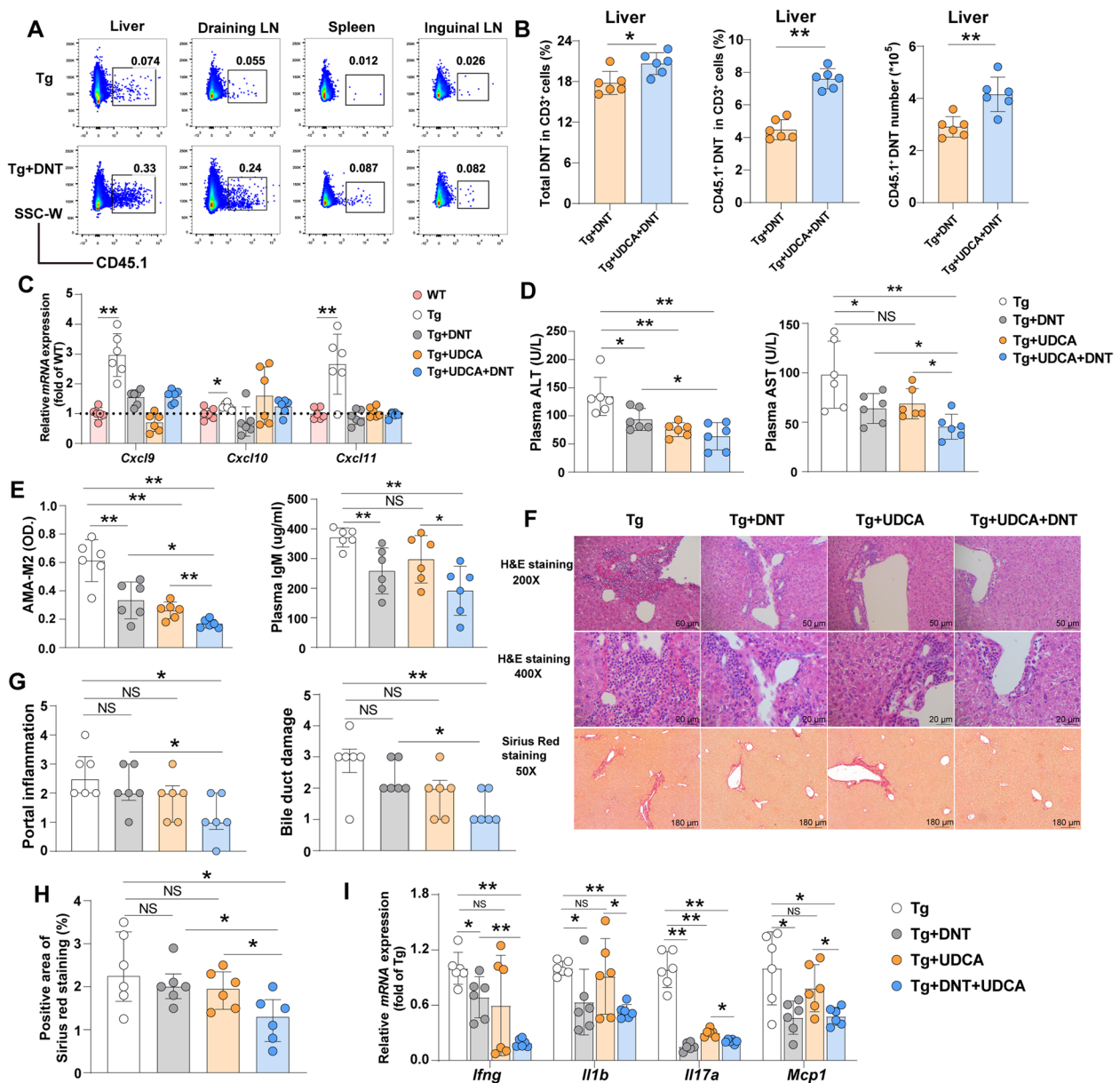


Fig. 1 Single DNT treatment alone or in combination with UDCA improved PBC. **A** Distribution of infused DNT in vivo. **B** (Left) Proportion of total intrahepatic DNT within the CD3⁺ cell population. (Middle) Proportion of CD45.1⁺ DNT relative to the CD3⁺ cell population. (Right) Quantitation of the number of infused DNT in the liver. **C** Relative mRNA levels of chemokines, including *Cxcl9*, *Cxcl10* and *Cxcl11*, in liver tissue. **D, E** Plasma ALT, AST, AMA-M2 and IgM levels. **F** Representative H&E (Hematoxylin & eosin) and Sirius red staining of liver paraffin sections. **G** Quantification of portal inflammation and bile duct damage in liver histology. **H** Quantification of the positive area of Sirius red staining in liver histology. **I** Relative mRNA expression levels associated with inflammation. *n* = 6 in each group. Statistical analysis for **G** (Right) was performed using the Kruskal-Wallis multiple comparisons test. Multiple comparisons were analyzed using one-way ANOVA followed by Bonferroni post hoc correction for normally distributed variables. **P* ≤ 0.05; ***P* ≤ 0.01; ALT, alanine transaminase; AMA-M2, antimitochondrial antibody M2; AST, aspartate transaminase; *Cxcl9*, C-X-C motif chemokine ligand 9; *Cxcl10*, C-X-C motif chemokine ligand 10; *Cxcl11*, C-X-C motif chemokine ligand 11; DNT, double-negative T cells; H&E, hematoxylin & eosin; *Ifng*, interferon-gamma; IgM, immunoglobulin M; *Il1b*, interleukin 1beta; *Il17a*, interleukin 17a; LN, lymph node; *Mcp1*, monocyte chemoattractant protein-1; Tg, dnTGFβRII mice; UDCA, ursodeoxycholic acid

treatment alone, combination therapy significantly decreased the positive area of Sirius red staining in dnTGFβRII mice (*p* = 0.022, *p* = 0.039, Fig. 1F and H).

As shown in Fig. 1I, DNT therapy dramatically decreased liver tissue *interferon-gamma* (*Ifng*), *interleukin 1beta* (*Il1b*), *monocyte chemoattractant protein-1*

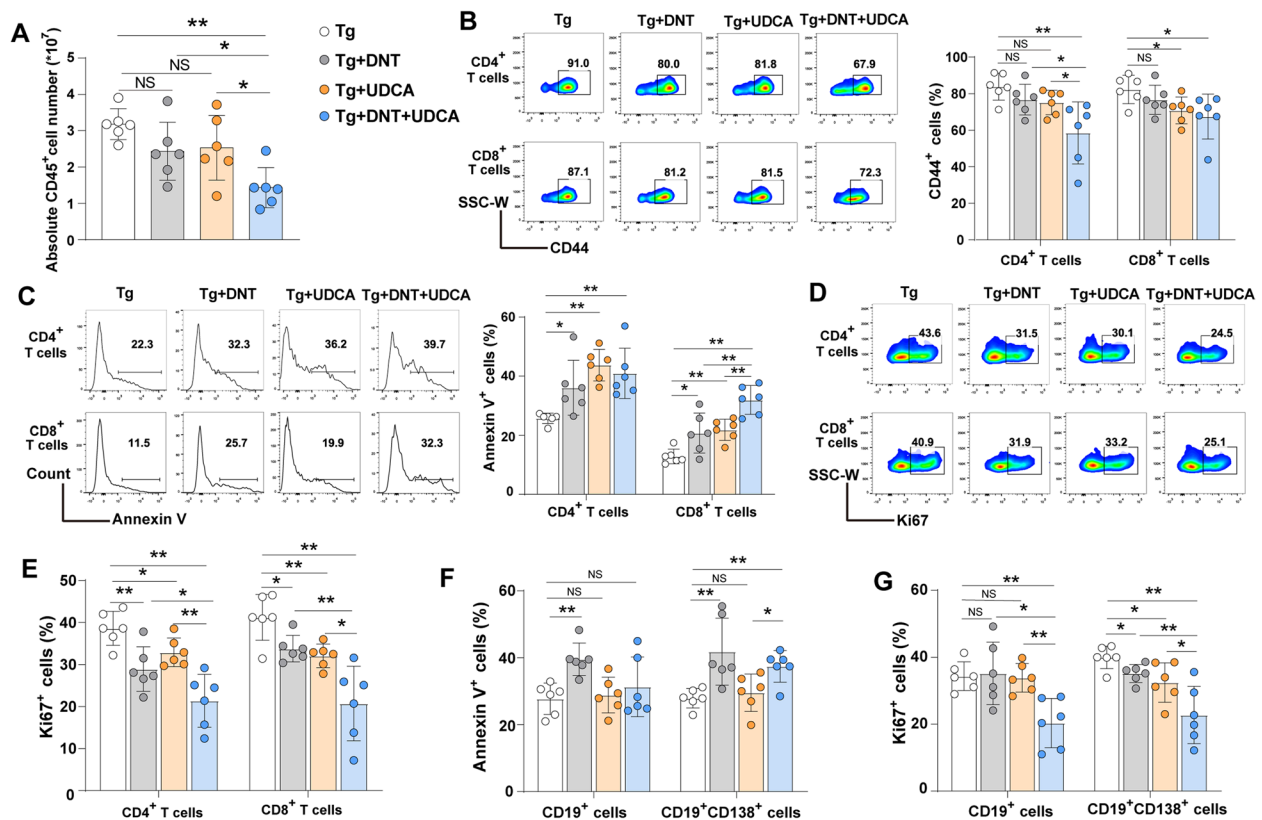


Fig. 2 DNT treatment alone or in combination with UDCA extensively inhibited T cells and B cells in vivo. **A** The absolute number of intrahepatic CD45⁺ cells. **B** Representative flow cytometry images and statistical analysis of intrahepatic CD44⁺CD4⁺ and CD44⁺CD8⁺ T cells. **C** Representative flow cytometry images and statistical analysis of Annexin V⁺ percentages in intrahepatic CD4⁺ and CD8⁺ T cells. **D** Representative flow cytometry images of Ki67⁺ liver CD4⁺ and CD8⁺ T cells. **E** Statistical analysis of Ki67⁺ percentages in intrahepatic CD4⁺ and CD8⁺ T cells. **F** Statistical analysis of Annexin V⁺ liver CD19⁺ B and CD19⁺CD138⁺ plasma cells, as determined by flow cytometry. **G** Statistical analysis of Ki67⁺ intrahepatic CD19⁺ B and CD19⁺CD138⁺ plasma cells, as determined by flow cytometry. $n=6$ in each group. Multiple comparisons were analyzed by one-way ANOVA followed by Bonferroni post hoc correction. * $P \leq 0.05$; ** $P \leq 0.01$. Tg, dnTGF β R1I mice; UDCA, ursodeoxycholic acid

(*Mcp1*) and *interleukin 17a* (*Il17a*) mRNA expression. In contrast, combination therapy not only reduced the levels of these proinflammatory cytokines but also further decreased *Ifng* mRNA expression. Similarly, combination therapy with DNT and UDCA improved protection against 2OA-BSA-immunized PBC (Additional file 3: Fig. S1). These results suggest that the transfer of DNT alone partly prevented the development of PBC, while combination therapy with UDCA significantly improved the histology, including liver fibrosis, in both dnTGF β R1I mice and 2OA-BSA-induced PBC mice.

To evaluate the long-term therapeutic effects of combined DNT and UDCA treatment, dnTGF β R1I mice were treated for 12 weeks. The combination therapy significantly improved plasma biomarkers of liver injury (ALT, AST, AMA-M2, and IgM), reduced portal inflammation and bile duct damage, and these improvements were sustained throughout the 12-week treatment period

(Additional file 3: Fig. S2A–D). Hepatic fibrosis, assessed by Sirius red staining, was also significantly reduced in mice receiving the combination therapy ($p=0.011$, Additional file 3: Fig. S2C and S2E). Furthermore, as the dnTGF β R1I mice used in this study also exhibited colitis, we assessed the impact of treatment on colon histology. DNT therapy alone significantly improved colon histology after 6–8 weeks ($p=0.043$), as evidenced by reduced inflammatory cell infiltration, decreased epithelial hyperplasia, and restoration of goblet cells (Additional file 3: Fig. S2E, G).

DNT in combination with UDCA inhibited lymphocyte proliferation and promoted lymphocyte apoptosis in vivo

In accordance with the gating strategy shown in Additional file 3: Fig. S3, we analyzed the subsets of lymphocytes by flow cytometry. As shown in Fig. 2A, DNT in combination with oral UDCA, but not UDCA

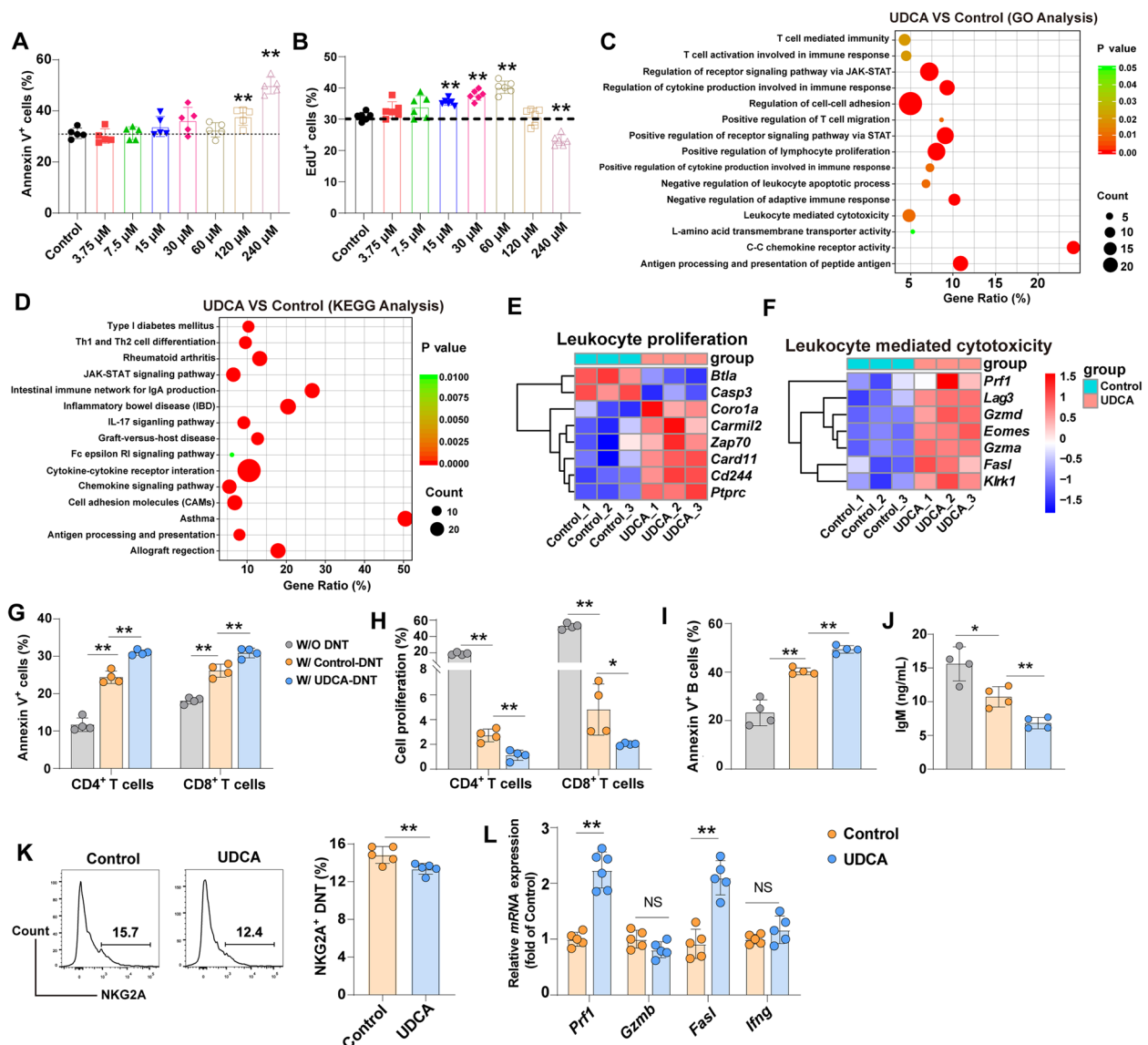


Fig. 3 UDCA augmented the immunosuppressive effect of DNT on T and B cells. Statistical analysis of Annexin V⁺ (A) and Edu⁺ DNT (B) cocultured with different concentrations of UDCA, as determined by flow cytometry ($n = 5$). Enriched GO (C) and KEGG (D) pathway analyses were performed on the significantly up- and downregulated genes in DNT. E Heatmap showing the up- and downregulated genes related to the regulation of leukocyte proliferation. F Heatmap showing the upregulated genes related to leukocyte-mediated cytotoxicity. G CD45.1-positive T cells were cocultured with control DNT or UDCA-stimulated DNT at a 4:1 ratio for 3 days in vitro. The apoptosis of CD4⁺ T cells and CD8⁺ T cells was detected by flow cytometry ($n = 4$). H Proliferation of CD4⁺ and CD8⁺ T cells, as determined by flow cytometry. I CD45.1-positive CD19⁺ B cells were cocultured with control DNT or UDCA-stimulated DNT at a 4:1 ratio for 3 days in vitro. Apoptosis of CD19⁺ B cells was detected by flow cytometry ($n = 4$). J The concentration of IgM in the supernatant of B cell cultures at 5 days ($n = 4$). K Representative flow cytometry images and statistical analysis of NKG2A⁺ DNT. L Relative levels of function-associated genes in DNT analyzed by quantitative real-time PCR. Experiments were repeated 2-3 times. Two-group comparisons were made via Student's t test, and multiple comparisons were analyzed by one-way ANOVA followed by Bonferroni post hoc correction. * $P \leq 0.05$; ** $P \leq 0.01$; NS, not significant. FasL, fas ligand; Gzmb, granzyme B; Ifng, interferon-gamma; NKG2A, also known as klrc1, killer cell lectin like receptor C1; Prf1, perforin 1; UDCA, ursodeoxycholic acid

monotherapy or DNT therapy alone, significantly reduced CD45-positive cell infiltration into the liver.

Combination therapy with DNT and UDCA reduced CD44 expression on CD4⁺ T cells and CD8⁺ T cells

(Fig. 2B). Moreover, all of the treatments induced the apoptosis of CD4⁺ T and CD8⁺ T cells, whereas combination therapy further increased the apoptosis of CD8⁺ T cells (Fig. 2C). Similarly, the proliferation of CD4⁺ T cells

and CD8⁺ T cells was significantly inhibited in all treatment groups, with the lowest proliferation rate observed in the combination therapy group (Fig. 2D and E).

In addition, we found that adoptive transfer of DNT had a strong killing effect on CD19⁺ B cells and CD19⁺CD138⁺ plasma cells (Fig. 2F and G), while combination therapy further inhibited the proliferation of B and plasma cells (Fig. 2F and G). These results suggested that the improvement in PBC caused by DNT treatment alone or in combination with UDCA may be due to the extensive inhibitory effects on liver-infiltrated lymphocytes.

UDCA augmented the immunosuppressive function of DNT

To further study the effects of UDCA on DNT, we stimulated DNT with or without UDCA for 48 h in vitro. As shown in Fig. 3A and B, UDCA concentrations ranging from 15 to 60 μ M did not prominently drive DNT apoptosis, but distinctly promoted their proliferation. Therefore, we used 60 μ M UDCA to further investigate its effects on DNT.

To further explore whether UDCA regulates the biological function of DNT, we analyzed the transcriptome data of DNT with or without UDCA stimulation. A total of 386 differentially expressed genes (DEGs) for GSE167116 were ultimately identified with an absolute $\log_2FC \geq 0.38$ and a P value ≤ 0.05 , and a volcano map of the DEGs is shown in Additional file 3: Fig. S4A. Gene Ontology (GO) categories (biological processes) and Kyoto Encyclopedia of Genes and Genomes (KEGG) pathway enrichment analyses revealed that the DEGs were involved mainly in T-cell-mediated immunity, regulation of cytokine production involved in the immune response, negative regulation of the adaptive immune response, C-C chemokine receptor activity, cytokine-cytokine receptor interaction and allograft rejection (Fig. 3C and D), which suggested that UDCA has extensive impacts on the biological functions of DNT.

As shown in Fig. 3E, compared with control DNT, DNT stimulated with UDCA exhibited upregulated expression of proliferation-promoting genes (*Coro1a*, *Carmil2*, *Zap70*, *Cd244*, *Ptprc*, and *Card11*) and down-regulated expression of antiproliferation genes (*Btla* and *Casp3*). More importantly, UDCA-stimulated DNT exhibited upregulation of genes involved in leukocyte-mediated cytotoxicity (*Prf1*, *Lag3*, *Gzmd*, *Eomes* and *Fasl*) (Fig. 3F). Consistently, we further confirmed these changes in related genes by real-time PCR (Additional file 3: Fig. S4B). These RNA sequencing data indicate that UDCA is involved in the anti-inflammatory response of DNT by promoting their proliferation and increasing their functional molecular expression.

We then verified the immunosuppressive effects of UDCA-stimulated DNT on T and B cells in vitro. CD4⁺ T cells and CD8⁺ T cells cocultured with DNT had increased apoptosis and decreased proliferation (Fig. 3G, H). Moreover, coculture with UDCA-stimulated DNT further increased apoptosis and strongly inhibited the proliferation of CD4⁺ T cells and CD8⁺ T cells (Fig. 3G, H). Similarly, B-cell apoptosis increased when B cells were cocultured with DNT, and the percentage of apoptotic B cells was further elevated in the UDCA-stimulated DNT coculture group (Fig. 3I). The level of IgM in the supernatant also decreased in the DNT group and was further reduced in the UDCA-stimulated DNT coculture group (Fig. 3J), indicating an enhanced inhibitory effect of UDCA-stimulated DNT on B cells.

As shown in Fig. 3K, UDCA markedly reduced the expression of NKG2A, an inhibitory molecule of DNT. Furthermore, UDCA also upregulated the mRNA expression of *Prf1* and *Fasl*, the key functional molecules of DNT (Fig. 3L). These results further indicated that UDCA could augment the suppressive effects of DNT on homologous cells via promotion of DNT proliferation and regulation of their functional molecule expression.

UDCA regulates the proliferation and function of DNT via FXR

To further verify the effect of UDCA on DNT, we detected several bile acid receptors expressed by DNT. As shown in Fig. 4A, only farnesoid X-activated receptor (*Fxr*) was significantly increased when DNT were stimulated with UDCA, suggesting that UDCA may regulate the function of DNT through FXR.

To further verify whether UDCA enhances the biological function of DNT via FXR, we utilized the FXR agonist obeticholic acid (OCA) and the FXR antagonist z-guggulsterone (GGS) to stimulate DNT. As depicted in Fig. 4B, exposure to UDCA increased the proliferation of DNT, which is consistent with the previous results. As anticipated, OCA also augmented the proliferation of DNT (Fig. 4B). Furthermore, the expression of NKG2A in DNT was notably reduced in the OCA group, consistent with the effect of UDCA on DNT (Fig. 4B). Similarly, the combination of UDCA and OCA promoted DNT proliferation and decreased the expression of the inhibitory receptor NKG2A (Fig. 4B). Additionally, DNT were pretreated with DMSO, UDCA, OCA, or UDCA + OCA for 3 days and then cocultured with CD45.1⁺ T cells for another 3 days. As shown in Fig. 4C, both UDCA and OCA enhanced DNT-mediated lysis of CD4⁺ T cells and CD8⁺ T cells, with similar outcomes observed in the UDCA + OCA group (Fig. 4C). These results indicated UDCA has effects on DNT, possibly relying on FXR.

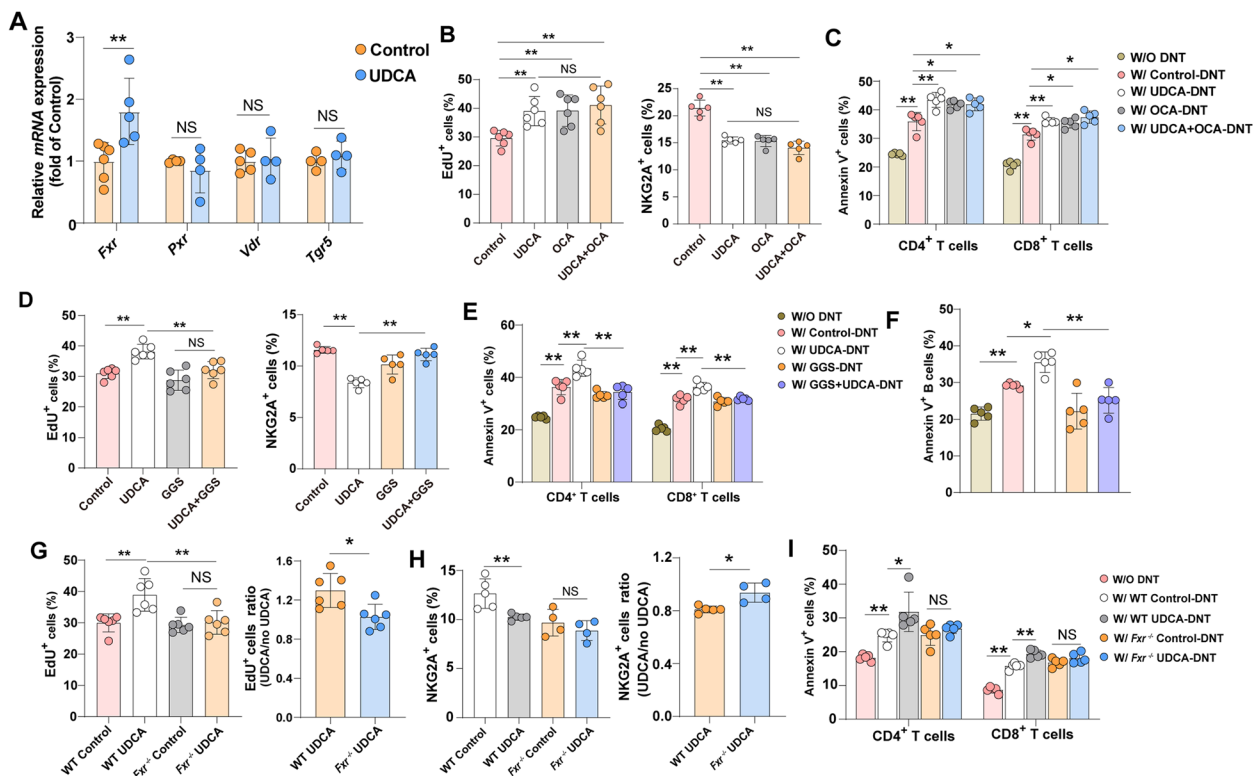


Fig. 4 UDCA regulated the proliferation and function of DNT via FXR. DNT were stimulated with DMSO (60 μ M), UDCA (60 μ M), OCA (0.5 μ M), UDCA (60 μ M) + OCA (0.5 μ M), GGS (5 μ M) or GGS (5 μ M) + UDCA (60 μ M) for 48 h. Then, we detected the proliferation and NKG2A expression of the DNT. In addition, we cocultured these stimulated DNT with CD45.1-positive T cells or B cells for another 3 days. **A** Relative levels of *Fxr*, *Pxr*, *Vdr* and *Tgr5* mRNAs in DNT, as analyzed by quantitative real-time PCR. **B** Statistical analysis of EdU⁺ and NKG2A⁺ cells relative to total DNT, as determined by flow cytometry ($n=5$). **C** Apoptosis of CD4⁺ and CD8⁺ T cells was detected by flow cytometry ($n=5$). **D** Statistical analysis of EdU⁺ and NKG2A⁺ cells relative to the total DNT. **E** The apoptosis of CD4⁺ and CD8⁺ T cells was detected by flow cytometry ($n=5$). **F** Statistical analysis of Annexin V⁺ B cells in each group ($n=5$). **G** Statistical analysis of EdU⁺ cells relative to the total number of WT DNT and *Fxr*^{-/-} DNT, as determined by flow cytometry (Left, $n=4$). Relative changes in the presence or absence of UDCA in WT DNT compared with *Fxr*^{-/-} DNT (Right). **H** Statistical analysis of NKG2A⁺ WT DNT and *Fxr*^{-/-} DNT, as determined by flow cytometry (Left, $n=4$). Relative changes in NKG2A in the presence or absence of UDCA in WT DNT compared with *Fxr*^{-/-} DNT (Right). **I** Apoptosis of CD4⁺ and CD8⁺ T cells was detected via flow cytometry ($n=4$). Experiments were repeated three times. Differences between two groups were analyzed via Student's t test, and multiple comparisons were analyzed by one-way ANOVA followed by Bonferroni post hoc correction. * $P \leq 0.05$; ** $P \leq 0.01$; NS, not significant. *Fxr*, farnesoid X receptor; *Fxr*^{-/-}, *Fxr* knockout; NKG2A, also known as *klrc1*, killer cell lectin like receptor C1; OCA, obeticholic acid; *Pxr*, pregnane X receptor; TNF- α , tumor necrosis factor alpha; *Tgr5*, g-protein coupled receptor 5; UDCA, ursodeoxycholic acid; *Vdr*, vitamin D receptor; GGS, z-guggulsterone

(See figure on next page.)

Fig. 5 UDCA regulated the proliferation and EPCR expression of DNT via the FXR/JNK pathway. WT and *Fxr*^{-/-} DNT were stimulated with anti-mouse CD3/CD28 antibodies with or without 60 μ M UDCA for 48h. **A** A total of 593 DEGs were identified between control WT DNT and UDCA-stimulated WT DNT. A total of 7402 non-DEGs were identified between control *Fxr*^{-/-} DNT and UDCA-stimulated *Fxr*^{-/-} DNT. Moreover, 907 DEGs were identified between WT DNT and *Fxr*^{-/-} DNT stimulated with UDCA. A Venn diagram revealed that these three datasets shared 22 genes. **B** Enriched GO pathway analyses were performed based on these 22 genes. **C** The FPKM level in DNT detected by RNA-seq. **D** Representative flow cytometry images and statistical analysis of the percentages of EPCR⁺ cells relative to total DNT, as quantified by flow cytometry. **E** Relative levels of *Epcr* mRNA in DNT analyzed by quantitative real-time PCR. **F** To detect the effect of EPCR, DNT were treated with WA (0.2 μ M, Cat#: HY-N2065, MCE) or UDCA (60 μ M) for 48 h. Statistical analysis of the percentages of EdU⁺ cells relative to the total DNT was performed, and the percentages were quantified by flow cytometry. **G** Relative levels of *Prf1*, *Gzmb* and *Klrc1* mRNAs in DNT were analyzed by quantitative real-time PCR. **H** Relative levels of *Jnk-1* and *Jnk-2* in DNT were analyzed by quantitative real-time PCR. **I, J** Representative flow cytometry images and statistical analysis of the level of p-JNK relative to total DNT, as quantified by flow cytometry. **K** Relative levels of *Epcr* mRNA in DNT were analyzed by quantitative real-time PCR. **L, M** Statistical analysis of the percentages of EPCR⁺ and EdU⁺ cells relative to total DNT, as quantified by flow cytometry. Experiments were repeated 2-3 times. Multiple comparisons were analyzed by one-way ANOVA followed by Bonferroni post hoc correction. * $P \leq 0.05$; ** $P \leq 0.01$; NS, not significant. DNT, double-negative T cells; EPCR, endothelial cell protein C receptor; FPKM, fragments per kilobase of exon model per million mapped fragments; *Fxr*^{-/-}, *Fxr* knockout; *Gzmb*, granzyme B; *Jnk*, c-Jun N-terminal kinase; JNK, c-Jun N-terminal kinase; JNK-IN8, JNK inhibitor XVI; *Klrc1*, killer cell lectin-like receptor C1; *Infg*, interferon-gamma; *Prf1*, perforin 1; UDCA, ursodeoxycholic acid; WA, withaferin A

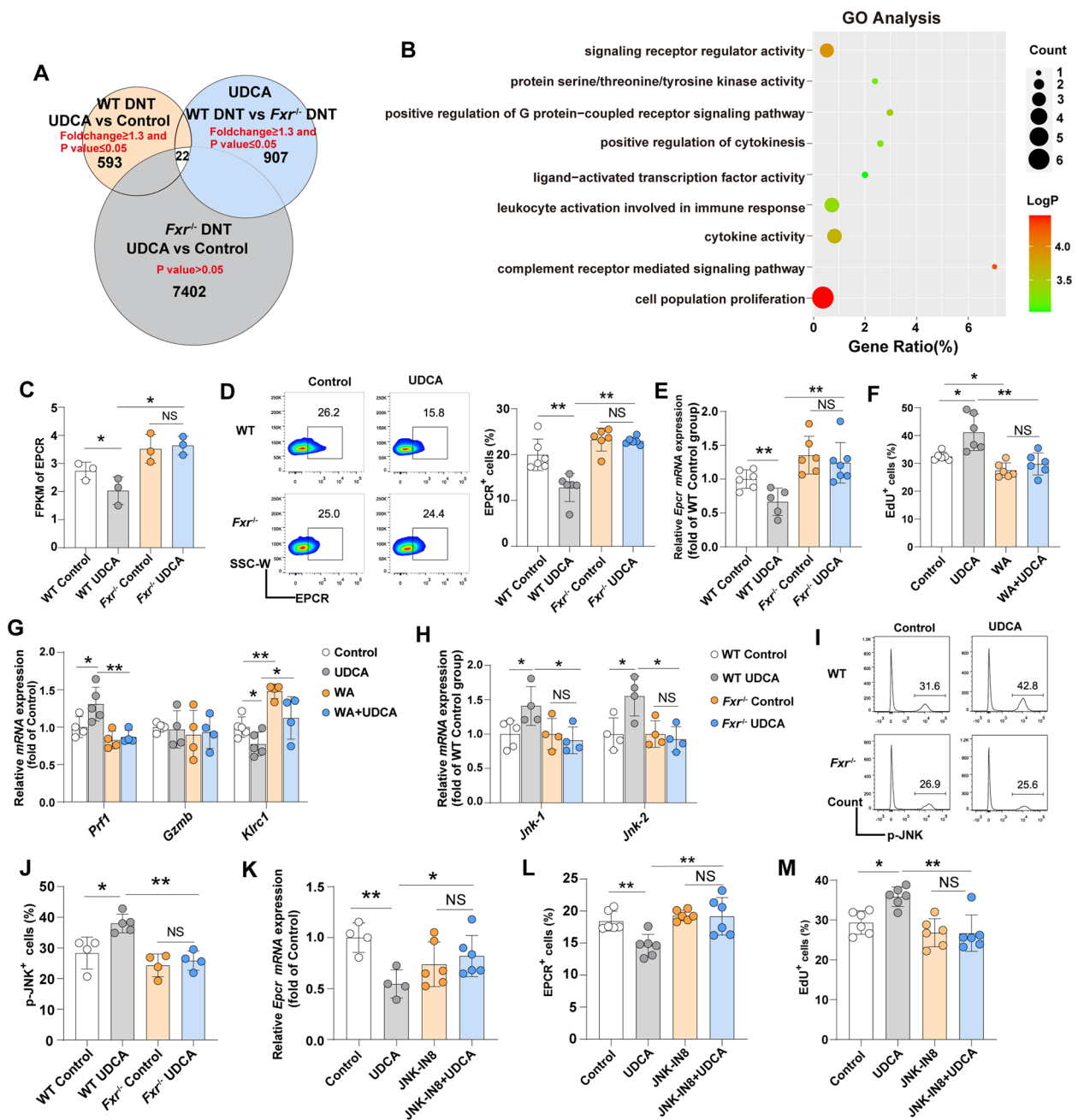


Fig. 5 (See legend on previous page.)

Furthermore, compared with UDCA, blocking the interaction of FXR with UDCA via GGS led to decreased proliferation and increased NKG2A expression in DNT (Fig. 4D). Moreover, as shown in Fig. 4E, the combination of UDCA and GGS significantly decreased the cytotoxicity of DNT toward CD4⁺ T cells and CD8⁺ T cells compared with UDCA alone. Similar results were observed in B cells (Fig. 4F). These results indicated that UDCA

enhanced the suppressive functions of DNT mainly through FXR.

To further confirm the effects of UDCA on DNT via FXR, we detected the expression of the proliferation-inhibiting molecule in WT and *Fxr*^{-/-} DNT after UDCA stimulation. As shown in Fig. 4G, consistent with the above results, UDCA significantly increased the proliferation of WT DNT but not *Fxr*^{-/-} DNT. Similarly, UDCA

decreased NKG2A expression in WT DNT, whereas UDCA had no such effect on *Fxr*^{-/-} DNT (Fig. 4H). WT DNT and *Fxr*^{-/-} DNT were pre-stimulated with DMSO or UDCA for 48 h and then cocultured with CD45.1⁺ T cells for another 3 days. Consistent with the above data, UDCA enhanced WT DNT-mediated CD4⁺ and CD8⁺ T cell lysis (Fig. 4I). However, UDCA did not increase the killing effect of *Fxr*^{-/-} DNT on CD4⁺ T cells or CD8⁺ T cells. These results further confirmed that UDCA enhanced the suppressive functions of DNT, mainly via FXR.

UDCA downregulated the expression of the inhibitory molecule endothelial cell protein C receptor (EPCR) in DNT through the FXR/JNK pathway

To explore how UDCA affects DNT via FXR, we analyzed the transcriptome data of WT DNT and *Fxr*^{-/-} DNT with or without UDCA. As shown in Fig. 5A, 593 DEGs were identified between control WT DNT and UDCA-stimulated WT DNT, while 907 DEGs were identified between control *Fxr*^{-/-} DNT and UDCA-stimulated *Fxr*^{-/-} DNT for GSE215278. Additionally, 7402 non-DEGs were identified between control *Fxr*^{-/-} DNT and UDCA-stimulated *Fxr*^{-/-} DNT. These three datasets contained 22 genes in common (Additional file 3: Fig. S4C), which were potentially critical for the FXR-dependent activation of DNT by UDCA. Gene Ontology (GO) categories revealed that these 22 genes were mainly involved in cell population proliferation, cytokine activity and leukocyte activation, which are involved in the immune response (Fig. 5B).

Among these 22 genes, protein C receptor (Procr, also known as EPCR), a coinhibitory receptor that is expressed on both CD4⁺ and CD8⁺ T cells and part of a larger coinhibitory gene program [15], was downregulated in WT DNT but not in *Fxr*^{-/-} DNT treated with UDCA (Fig. 5C). These findings were further validated at both the mRNA and protein levels (Fig. 5D and E).

To further confirm the biological roles of EPCR, withaferin A (WA), an agonist of EPCR, was used in this study. As shown in Fig. 5F, WA significantly inhibited the proliferation of DNT and prevented the effect of UDCA on DNT, indicating that EPCR acts as an inhibitory molecule of DNT. Consistently, WA not only reduced *Prf1* mRNA expression and increased *Klrc1* (NKG2A) mRNA expression but also reversed the effects of UDCA on DNT (Fig. 5G).

According to a previous study, EPCR is regulated by the JNK signaling pathway [16]. In our study, Fig. 5H shows that both *Jnk-1* and *Jnk-2* mRNAs were upregulated in UDCA-stimulated WT DNT but not in *Fxr*^{-/-} DNT. Consistently, flow cytometry analysis revealed that the phosphorylation of JNK was significantly

increased in WT DNT stimulated with UDCA but not in *Fxr*^{-/-} DNT (Fig. 5I, J).

To further explore whether EPCR is regulated by the JNK pathway in DNT, the JNK inhibitor JNK-IN8 (1 μM) was used to block the JNK signaling pathway. As shown in Fig. 5K, *Epcr* mRNA was reduced in UDCA-stimulated DNT, while its expression was reversed in DNT treated with JNK-IN8 in combination with UDCA. Moreover, JNK-IN8 prevented EPCR expression and the regulation of DNT proliferation by UDCA (Fig. 5L, M). These results suggested that UDCA promoted proliferation and downregulated the expression of the inhibitory molecule EPCR in DNT through the FXR/JNK signaling pathway.

UDCA enhanced the therapeutic role of DNT in vivo

To verify the mechanism by which UDCA regulates DNT in vivo, we transferred CD45.1⁺ DNT into dnTGFβRII mice with or without UDCA intragastric administration for 1 week (Fig. 6A). We found that these DNT still maintained a stable phenotype of CD3⁺NK1.1⁻CD4⁻CD8⁻ in vivo (Additional file 3: Fig. S4D). As shown in Fig. 6B, combination therapy with UDCA significantly increased the percentage of CD45.1⁺ DNT in the liver. Consistent with the above results, combination therapy with UDCA had no effect on the apoptosis of infused DNT but significantly promoted their proliferation (Fig. 6B, C). Moreover, compared with DNT therapy alone, UDCA also decreased the levels of the inhibitory molecule NKG2A but had no effect on granzyme B expression in transferred DNT (Fig. 6D). Consistent with the in vitro observations, combination therapy with UDCA increased FXR expression of DNT (Fig. 6E, F). Additionally, UDCA downregulated EPCR expression of transferred DNT and upregulated the JNK signal (Fig. 6G). These results further suggested that combination therapy with UDCA increased DNT proliferation and downregulated the expression of the inhibitory molecule NKG2A/EPCR in DNT through the FXR/JNK signaling pathway.

UDCA promotes the proliferation and immunoregulatory function of human DNT via the FXR/JNK/EPCR pathway

To further investigate whether UDCA regulates DNT proliferation and function via the FXR/JNK signaling pathway, we performed in vitro experiments using human DNT. As shown in Fig. 7A, consistent with previous findings in mice, UDCA upregulated the mRNA expression of *Prf1*, *Gzmb* and *Fasf* and decreased the expression of the exhaustion marker *Klrc1*. Moreover, UDCA significantly increased the protein levels of perforin and granzyme B and significantly promoted human DNT proliferation (Fig. 7B). Furthermore, in contrast to those in the cocultures with control DNT, the number of apoptotic CD4⁺ T cells, CD8⁺ T cells and CD19⁺ B

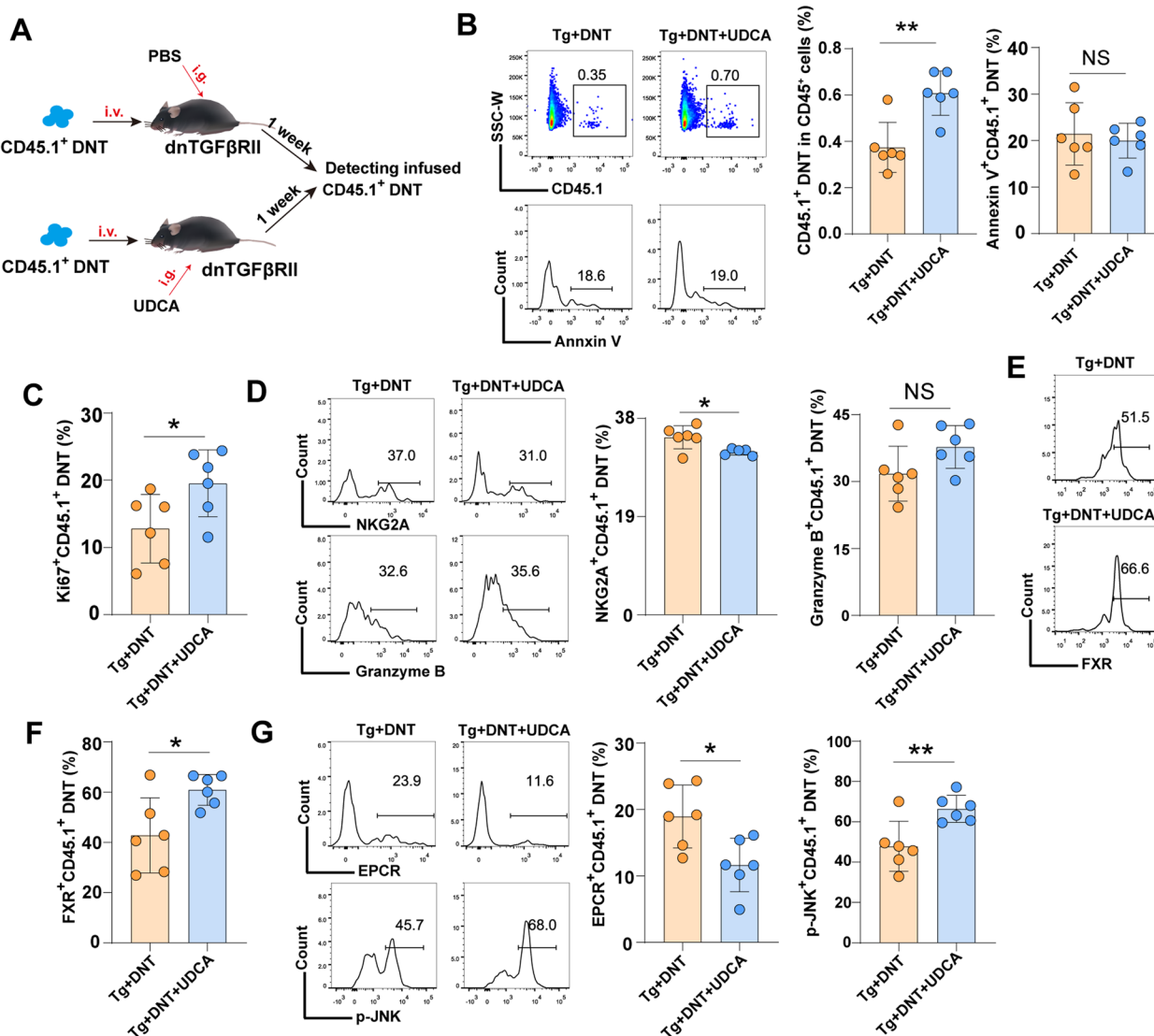


Fig. 6 UDCA enhanced the therapeutic role of DNT in vivo. **A** Flowchart showing that 6–8-week-old dnTGFβRII mice received a total of 3×10^6 CD45.1-positive DNT via tail vein injection. At the same time, UDCA (15 mg/kg/day) was administered daily by intragastric administration for 1 week ($n=6$). **B** Representative flow cytometry images and statistical analysis of transferred CD45.1⁺ DNT in total hepatic CD45⁺ cells. Representative flow cytometry images and statistical analysis of Annexin V⁺ cells relative to the total CD45.1-positive DNT. **C** Statistical analysis of Ki67⁺ cells relative to the total CD45.1-positive DNT, as determined by flow cytometry. **D** Representative flow cytometry images and statistical analysis of NKG2A⁺ and granzyme B⁺ cells relative to the total CD45.1-positive DNT. **E, F** Representative flow cytometry images and statistical analysis of FXR⁺ cells relative to the total CD45.1-positive DNT. **G** Representative flow cytometry images and statistical analysis of EPCR⁺ or p-JNK⁺ cells relative to the total CD45.1-positive DNT. Two-group comparisons were made by Student's t test followed by Bonferroni post hoc correction. * $P \leq 0.05$; ** $P \leq 0.01$; NS, not significant. DNT, double-negative T cells; FXR, farnesoid X receptor; EPCR, endothelial cell protein C receptor; JNK, c-Jun N-terminal kinase; NKG2A, also known as klrc1, killer cell lectin like receptor C1; Tg, dnTGFβRII mice; UDCA, ursodeoxycholic acid

cells cocultured with UDCA-stimulated DNT was much greater (Fig. 7C), indicating that the cytotoxic activity of DNT was enhanced by UDCA.

UDCA also dramatically upregulated *Fxr* and *vitamin D receptor (Vdr)* expression in human DNT (Fig. 7D). We further investigated the increase in FXR expression by human DNT via flow cytometry (Fig. 7E). Consistent

with the previous results, UDCA decreased EPCR expression by human DNT (Fig. 7F).

To further confirm the biological roles of EPCR in human DNT, WA was used in this study. As shown in Fig. 7G, WA not only significantly inhibited the proliferation of DNT and prevented the UDCA-induced effects on DNT but also decreased perforin expression by DNT,

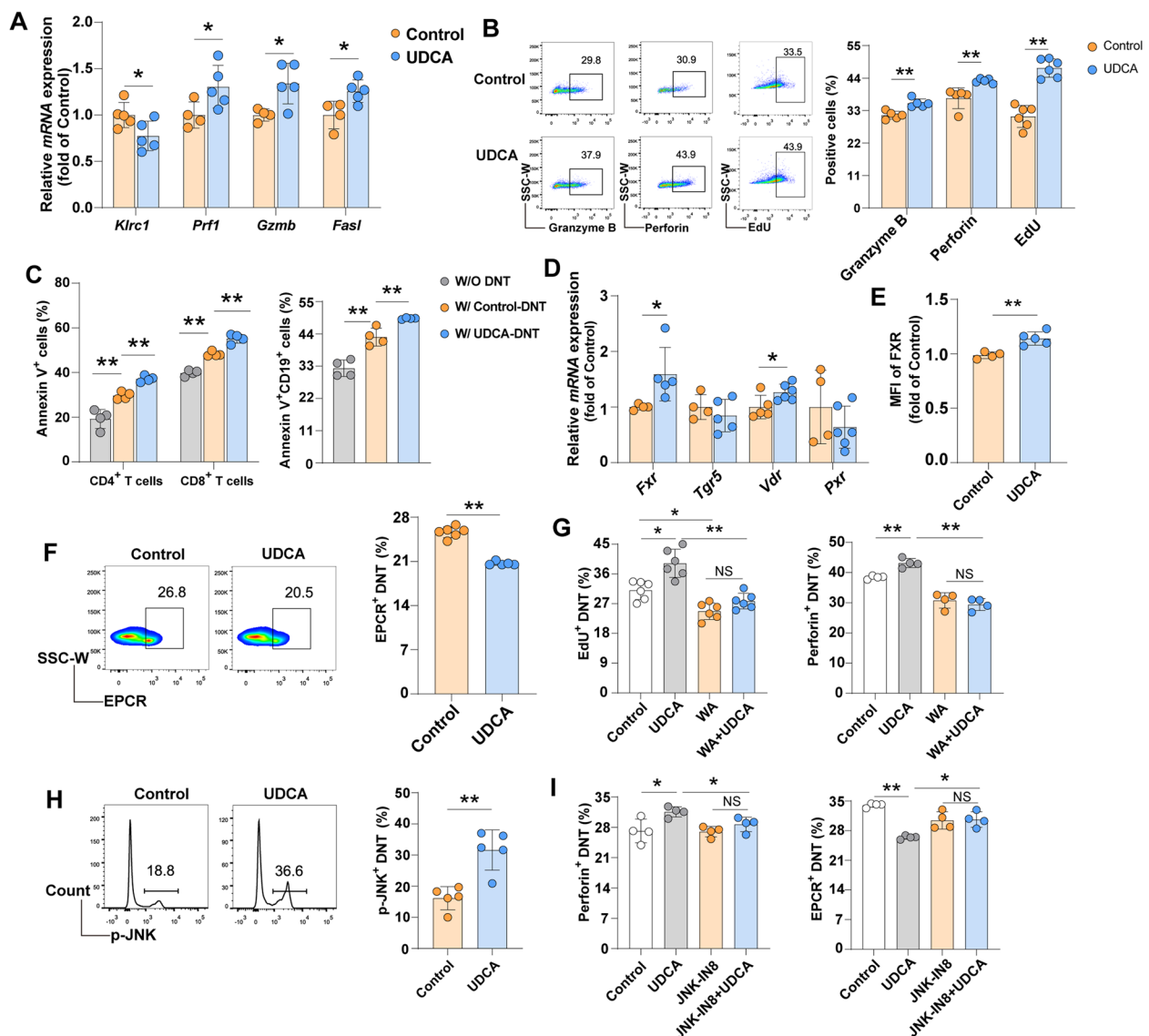


Fig. 7 UDCA also regulates human DNT proliferation and immunoregulatory functions. **A** Relative levels of function-associated genes in human DNT analyzed by quantitative real-time PCR. **B** Representative flow cytometry images and statistical analysis of the percentages of perforin⁺, granzyme B⁺ and Edu⁺ cells relative to the total DNT, as quantified by flow cytometry. **C** T or B cells were cocultured with control DNT or UDCA-stimulated DNT at a 5:1 ratio for 1 day in vitro. The apoptosis of CD4⁺ and CD8⁺ T cells (left) and CD19⁺ cells (right) was detected by flow cytometry ($n=4$). **D** Relative levels of *Fxr*, *Pxr*, *Vdr* and *Tgr5* mRNAs in DNT, as analyzed by quantitative real-time PCR. **E** The mean fluorescence intensity (MFI) of FXR on DNT quantified by flow cytometry. **F** Representative flow cytometry images and statistical analysis of the percentages of EPCR⁺ cells relative to the total DNT. **G** To detect the effects of EPCR, human DNT were treated with WA (0.2 μ M) or UDCA (60 μ M) for 48 h. Statistical analysis of the percentages of Edu⁺ cells and perforin⁺ cells relative to the total DNT was performed, and the percentages were quantified via flow cytometry. **H** Representative flow cytometry images and statistical analysis of the percentages of p-JNK⁺ cells relative to the total DNT, as quantified by flow cytometry. **I** Statistical analysis of the percentages of perforin⁺ and EPCR⁺ cells relative to the total DNT, as quantified by flow cytometry. $n=4-6$ per group. Experiments were repeated 2-3 times. Two-group comparisons were made via Student's t test, and multiple comparisons were analyzed by one-way ANOVA followed by Bonferroni post hoc correction. * $P \leq 0.05$; ** $P \leq 0.01$; NS, not significant. DNT, double-negative T cells; EPCR, endothelial cell protein C receptor; Fas1, fas ligand; Fxr, farnesoid X receptor; Gzmb, granzyme B; Infg, interferon-gamma; JNK, c-Jun N-terminal kinase; Klrc1, killer cell lectin like receptor C1; Prf1, perforin 1; Pxr, pregnane X receptor; Tgr5, g-protein coupled receptor 5; UDCA, ursodeoxycholic acid; Vdr, vitamin D receptor; WA, withaferin A

indicating that EPCR acts as an inhibitory molecule of human DNT. Moreover, UDCA increased JNK phosphorylation in human DNT (Fig. 7H). JNK-IN8, a JNK pathway inhibitor, prevented the UDCA-mediated regulation of perforin and EPCR expression in human DNT (Fig. 7I). These results demonstrated that UDCA could augment the suppressive function of human DNT via the FXR/JNK/EPCR pathway, consistent with the observations in mice.

Discussion

DNT play diverse and distinct roles in various diseases. A previous study reported that DNT have dual pathogenic and therapeutic effects on autoimmune diseases [17]. Studies have shown that DNT exhibit traits associated with resistance to autoimmune diabetes, and DNT infusion significantly reduces the diabetes incidence and prevents the progression of type 1 diabetes (T1D) [18–20]. However, in contrast to the therapeutic potential of DNT in T1D, DNT have been implicated as a harbinger of systemic lupus erythematosus (SLE) and primary Sjögren's syndrome (pSS). These expanded DNT produce increased levels of IL-17 and IFN- γ , contributing to the progression of SLE and pSS progression [21–24]. In conclusion, further studies are needed to explore the intricate mechanisms underlying these contrasting roles of DNT in different autoimmune contexts.

In this study, we found that adoptive transfer of ex vivo-generated DNT potently protected against PBC by suppressing liver-infiltrating T and B cells in mice. The combination therapy of DNT and UDCA exhibited better therapeutic efficacy, with markedly improved liver inflammation and stronger inhibition of hepatic T cells and B cells. Furthermore, UDCA augmented the immunosuppressive function of DNT via FXR.

The transferred DNT primarily infiltrated the liver and draining lymph nodes. This may be due to the high concentration of chemokines (CXCL10/CXCL9) in the liver, which facilitate the migration of DNT and the subsequent high expression of the chemokine receptor CXCR3 [25]. In our previous studies, the cytotoxicity of DNT was shown to depend mainly on functional molecules, such as perforin and granzyme B [5, 25]. Moreover, DNT were also verified to directly lyse B cells through cell-cell contact via perforin [26]. These effects may be the major mechanisms by which these infused DNT inhibited CD4⁺ and CD8⁺ T cells and B cells, resulting in the amelioration of PBC in mice.

Our in vitro experiments further verified that UDCA promoted proliferation and reduced inhibitory molecule expression in DNT via FXR. However, the interplay between UDCA and FXR is controversial. UDCA can act as both a weak FXR agonist and a FXR antagonist [27]. A

recent study showed that UDCA could reduce FXR signaling and downregulate ACE2 in human lung, cholangiocyte and intestinal organoids [28]. Moreover, as a weaker ligand of FXR [29], UDCA can bind to FXR in hepatocytes [30]. Previous studies also reported that UDCA acts as a partial agonist of FXR and regulates the expression of the ileal bile acid binding protein (IBABP) in the liver [31]. The administration of a mixture of lithocholic acid and UDCA reduces hyperlipidemia by activating the FXR pathway and repairing gut barrier integrity in *ob/ob* mice [32]. Furthermore, UDCA has the ability to bind to FXR in hepatocytes at high concentrations [30]. Recent studies have revealed that UDCA can upregulate the expression of FXR in intestinal tissues [33, 34]. However, the interaction between UDCA and FXR in DNT deserves further study.

UDCA has been reported to have anti-inflammatory, immunomodulatory and antiapoptotic effects [27]. Many studies have demonstrated that UDCA can protect hepatocytes from alcohol or toxic bile acids and reduce oxygen species (ROS) production through FXR [35]. Additionally, UDCA also plays immunomodulatory roles. Treatment with UDCA for 4 weeks inhibited the function of dendritic cells in an ovalbumin (OVA)-driven eosinophilic airway inflammation model [36]. UDCA also profoundly reduced IL-2 and IFN- γ expression in a PBC mouse model [37].

FXR belongs to the nuclear receptor superfamily and is a ligand-activated transcription factor that plays an important role in regulating bile acid levels, lipid homeostasis, and glucose metabolism [38]. In addition, FXR has been detected extensively in innate (including macrophages, NK cells and dendritic cells) and adaptive immune cells (including CD4⁺ and CD8⁺ T cells) [39], and strongly affects these cells [40]. Once activated, FXR reduces the macrophage response to proinflammatory stimuli, exerting a counterregulatory signal [41]. Moreover, FXR activation drives the accumulation of myeloid-derived suppressor cells (MDSCs) in ConA-induced liver injury and enhances their suppressor function by binding to the paired immunoglobulin-like receptor-B promoter [42]. However, the downstream signals of FXR in DNT remain unknown.

In our study, we found that the expression level of EPCR in DNT was modulated by FXR. EPCR, also known as PROC1, is a transmembrane protein that plays a critical role in the activated protein C (APC)-mediated anticoagulant pathway [43]. Furthermore, studies have suggested that EPCR is a key protein that supports APC-induced cytoprotective signaling through the activation of protease-activated receptors [44, 45]. Another study reported that free fatty acids could inhibit EPCR expression in endothelial cells through the activation of

JNK signaling [16]. In line with these previous studies, we showed UDCA could counteract the inhibitory effect of an EPCR agonist on the proliferation of DNT, probably through activation of the JNK pathway and inhibition of EPCR expression.

Additionally, another study revealed that adoptive transfer of DNT could augment the accumulation of recipient Tregs, thereby contributing to long-term cardiac allograft survival [46]. Furthermore, the transfer of DNT enhances Treg recruitment, fostering an immune homeostatic environment conducive to neuronal recovery in ischemic stroke [47]. Unfortunately, in our study, we did not detect any changes in Tregs during DNT treatment.

While the combined DNT and UDCA treatment demonstrated promising results in both dnTGF β R11 and 2OA-BSA-immunized mice, we acknowledge certain limitations. First, expanding our investigation to include a broader range of PBC models is essential. Although we employed two distinct models, neither fully recapitulates the female predominance characteristic of human PBC, nor do they exhibit the severe bile duct inflammation often observed clinically. The ARE-Del^{-/-} mouse model has been shown to accurately reflect several key features of human PBC [48–50], and we plan to utilize this model for future validation once it becomes accessible. Second, the development and application of a *bona fide* humanized PBC mouse model are critical for a more comprehensive assessment of the safety and potential long-term effects of DNT therapy.

We also verified that UDCA promoted human DNT proliferation and increased the expression of functional molecules in human DNT, including perforin and granzyme B. Furthermore, we demonstrated that UDCA profoundly increased FXR, activated the JNK pathway and reduced EPCR expression by human DNT. However, the detailed mechanism of FXR activation in DNT needs further in-depth exploration in the future.

In conclusion, the transfer of DNT in combination with oral UDCA ameliorated PBC in mice by inhibiting hepatic T cells and B cells. UDCA promoted DNT proliferation and reduced EPCR expression, thereby augmenting the suppressive function of DNT via the FXR/JNK signaling pathway. Our study hopes to provide a potential application of DNT-based combination therapy for PBC patients who are nonresponsive to UDCA.

Conclusions

In summary, our study underlies that a single transfer of DNT ameliorated PBC in mice, while combination therapy of DNT with oral UDCA displayed a better efficacy with stronger inhibition of hepatic T and B cells. Moreover, UDCA promoted DNT proliferation and reduced

EPCR expression, thereby augmenting the suppressive function of DNT via the FXR/JNK signaling pathway. This study provides a potential application of DNT-based combination therapy for PBC, especially for UDCA non-responders.

Abbreviations

ALP	Alkaline phosphatase
ALT	Alanine transaminase
AMA-M2	Antimitochondrial antibody M2
AST	Aspartate transaminase
CFA	Complete Freund's adjuvant
CFSE	Carboxyfluorescein diacetate succinimidyl ester
DMSO	Dimethyl sulfoxide
DNT	Double-negative T cells
EdU	5-Ethynyl-2'-deoxyuridine
FXR	Farnesoid X receptor
GGS	Z-guggulsterone
H&E	Hematoxylin & eosin
IFA	Incomplete Freund's adjuvant
Igng	Interferon-gamma
IgM	Immunoglobulin M
IL1b	Interleukin 1beta
IL17a	Interleukin 17a
I.P.	Intraperitoneally
JNK-IN8	JNK inhibitor XVI
Mcp1	Monocyte chemoattractant protein-1
OCA	Obeticholic acid
PBC	Primary biliary cholangitis
PCR	Polymerase chain reaction
PROCR	(Also known as EPCR, endothelial cell protein C receptor): protein C receptor
Tg	DnTGF β R11 mice
UDCA	Ursodeoxycholic acid
Vdr	Vitamin D receptor
WA	Withaferin A
WT	Wild-type

Supplementary Information

The online version contains supplementary material available at <https://doi.org/10.1186/s12916-025-04043-9>.

Additional file 1: The ARRIVE guidelines.

Additional file 2: Table S1. List of primers used in the experiment.

Additional file 3: Fig S1. DNT treatment combined with UDCA significantly prevented the development of PBC in 2OA-BSA immunized mice. A-E. Plasma ALT, AST, AMA-M2, IgM, IgG and ALP were measured. F. Representative H&E and Sirius red staining in liver paraffin sections. G. Quantification of portal inflammation by liver histology staining. H. Quantification of bile duct damage in liver histology staining. I. Quantification of positive area of Sirius red staining in liver histology. J. Relative levels of proinflammatory cytokine mRNA in liver tissue analyzed by quantitative real-time PCR. $n = 5-6$ in each group. Fig S2. Duration of therapeutic effects of combined DNT and UDCA treatment and effects of DNT on colitis in dnTGF β R11 (Tg) mice. A-B. Plasma levels of ALT, AST, AMA-M2, and IgM over a 12-week treatment period. C. Representative H&E and Sirius red staining of liver paraffin sections. D. Quantification of portal inflammation and bile duct damage. E. Quantification of the Sirius red-positive area in liver sections. F. Representative H&E staining of colon paraffin sections. G. Quantification of colitis in colon sections. $n = 10$ per group. Fig S3. Gating strategy for analyzing the cell subsets of intrahepatic monocytes. A. Representative flow cytometry gating strategy to analyze the subsets of T cells. B. Representative flow cytometry gating strategy to analyze liver B cells (CD19⁺) and plasma cells (CD19⁺CD138⁺). Fig S4. The regulation of UDCA on DNT. A. Mouse DNT were stimulated by anti-mouse CD3/CD28 antibodies with or without 60 μ M UDCA. Volcano map showing the distributions of up- and

downregulated genes (differentially expressed genes identified by the fold change of ≥ 0.5 and $P \leq 0.05$) in DNT from the above two groups. B. The genes associated with lymphocyte proliferation and cell cytotoxicity were confirmed in DNT by real-time PCR after UDCA stimulation ($n = 5$). C. The heat map displayed these 22 genes, which included *Epcr*. D. Representative flow cytometry gating strategy to analyze the CD45.1⁺CD3⁺NK1.1⁻CD4⁺CD8⁻ DNT in liver.

Acknowledgements

Not applicable.

Authors' contributions

All listed authors participated meaningfully in the study and have read and approved the submission of this manuscript. C.Z. and G.S. participated in performing the research, analyzing the data, and writing the original draft of the article. H. J, Y.W., S.Z., X.W. and X.Z. participated in performing the research and collecting the data. D.Z. established the hypothesis, supervised the studies, analyzed the data, and cowrote the manuscript. J.J. participated in developing the hypothesis and in the review and editing of the manuscript.

Funding

This study was supported by grants from the National Natural Science Foundation of China (81770598, 81970503, and 82270606), the Beijing Natural Science Foundation (7244319), the R&D Program of Beijing Municipal Education Commission KZ202210025036, Beijing Municipal Administration of Hospitals' Ascent Plan DFL20220103 and Youth Beijing Scholar (No. 035).

Data availability

All data and materials supporting the findings of this manuscript are presented in the paper and/or the supplemental information. The mRNA sequencing data reported in this work have been uploaded to the National Center for Biotechnology Information (NCBI) Gene Expression Omnibus (GEO) database under accession numbers GSE167116 (<https://www.ncbi.nlm.nih.gov/geo/query/acc.cgi?acc=GSE167116>) and GSE215278 (<https://www.ncbi.nlm.nih.gov/geo/query/acc.cgi?acc=GSE215278>). The analyzed data sets generated during the study are available from the corresponding author on reasonable request.

Declarations

Ethics approval and consent to participate

The human DNT study was approved by the Research Ethics Committee of Beijing Friendship Hospital under ethics approval number 2020-P2-196-02, and informed consent from all healthy volunteers was obtained. All of the mice were housed and maintained in a pathogen-free, temperature-controlled environment at the Beijing Friendship Hospital under approval number 21-2011 for animal housing and use. All experimental procedures were conducted in accordance with the protocol approved by the Institutional Animal Care and Ethics Committee at Beijing Friendship Hospital and with the National Institutes of Health guidelines for the care and use of laboratory animals.

Consent for publication

All authors read and approved the manuscript.

Competing interests

The authors declare no competing interests.

Author details

¹Liver Research Center, Beijing Friendship Hospital, Capital Medical University, Beijing 100050, China. ²State Key Lab of Digestive Health, Beijing Friendship Hospital, Capital Medical University, Beijing 100050, China. ³National Clinical Research Center for Digestive Disease, Beijing 100050, China. ⁴Medical Research Center, Beijing Chao-Yang Hospital, Capital Medical University, No. 8 South Gongti Road, Beijing 100020, China. ⁵Department of Gastroenterology, Beijing Chao-Yang Hospital, Capital Medical University, Beijing 100020, China. ⁶General Surgery Department, Beijing Friendship Hospital, Capital Medical University, Beijing 100050, China. ⁷Beijing Laboratory of Oral Health, Capital Medical University School of Basic Medicine, Beijing 100069, China.

Received: 3 November 2024 Accepted: 27 March 2025

Published online: 07 April 2025

References

- Carbone M, Sharp SJ, Flack S, Paximadas D, Spiess K, Adgey C, et al. The UK-PBC risk scores: Derivation and validation of a scoring system for long-term prediction of end-stage liver disease in primary biliary cholangitis. *Hepatology*. 2016;63:930–50.
- Mayo MJ. Mechanisms and molecules: What are the treatment targets for primary biliary cholangitis? *Hepatology*. 2022;76:518–31.
- Melchor-Mendoza YK, Martinez-Benitez B, Mina-Hawat A, Rodriguez-Leal G, Duque X, Moran-Villota S. Ursodeoxycholic acid therapy in patients with primary biliary cholangitis with limited liver transplantation availability. *Ann Hepatol*. 2017;16:430–5.
- Brandt D, Hedrich CM. TCR $\alpha\beta$ (+)-CD3(+)-CD4(-)-CD8(-) (double negative) T cells in autoimmunity. *Autoimmun Rev*. 2018;17:422–30.
- Zhang D, Yang W, Degauque N, Tian Y, Mikita A, Zheng XX. New differentiation pathway for double-negative regulatory T cells that regulates the magnitude of immune responses. *Blood*. 2007;109:4071–9.
- Velikkakam T, Gollob KJ, Dutra WO. Double-negative T cells: Setting the stage for disease control or progression. *Immunology*. 2022;165:371–85.
- Wu Z, Zheng Y, Sheng J, Han Y, Yang Y, Pan H, et al. CD3(+)-CD4(-)-CD8(-) (Double-Negative) T Cells in Inflammation Immune Disorders and Cancer. *Front Immunol*. 2022;13:816005.
- Tian D, Yang L, Wang S, Zhu Y, Shi W, Zhang C, et al. Double negative T cells mediate Lag3-dependent antigen-specific protection in allergic asthma. *Nat Commun*. 2019;10:4246.
- Sun G, Zhao X, Li M, Zhang C, Jin H, Li C, et al. CD4 derived double negative T cells prevent the development and progression of nonalcoholic steatohepatitis. *Nat Commun*. 2021;12:650.
- Li SX, Lv TT, Zhang CP, Wang TQ, Tian D, Sun GY, et al. Alteration of liver-infiltrated and peripheral blood double-negative T-cells in primary biliary cholangitis. *Liver Int*. 2019;39:1755–67.
- Ouyang H, Mei X, Zhang T, Lu B, Ji L. Ursodeoxycholic acid ameliorates diabetic retinopathy via reducing retinal inflammation and reversing the breakdown of blood-retinal barrier. *Eur J Pharmacol*. 2018;840:20–7.
- Zhao ZB, Lu FT, Ma HD, Wang YH, Yang W, Long J, et al. Liver-resident NK cells suppress autoimmune cholangitis and limit the proliferation of CD4⁺ T cells. *Cell Mol Immunol*. 2020;17:178–89.
- Yang W, Yao Y, Yang YQ, Lu FT, Li L, Wang YH, et al. Differential modulation by IL-17A of Cholangitis versus Colitis in IL-2Ralpha deleted mice. *PLoS One*. 2014;9:e105351.
- Ando Y, Yang GX, Tsuda M, Kawata K, Zhang W, Nakajima T, et al. The immunobiology of colitis and cholangitis in interleukin-23p19 and interleukin-17A deleted dominant negative form of transforming growth factor beta receptor type II mice. *Hepatology*. 2012;56:1418–26.
- Chihara N, Madi A, Kondo T, Zhang H, Acharya N, Singer M, et al. Induction and transcriptional regulation of the co-inhibitory gene module in T cells. *Nature*. 2018;558:454–9.
- Xie W, Zhai Z, Yang Y, Kuang T, Wang C. Free fatty acids inhibit TM-EPICR expression through JNK pathway: an implication for the development of the prothrombotic state in metabolic syndrome. *J Thromb Thrombolysis*. 2012;34:468–74.
- Li H, Tsokos GC. Double-negative T cells in autoimmune diseases. *Curr Opin Rheumatol*. 2021;33:163–72.
- Liu T, Cong M, Sun G, Wang P, Tian Y, Shi W, et al. Combination of double negative T cells and anti-thymocyte serum reverses type 1 diabetes in NOD mice. *J Transl Med*. 2016;14:57.
- Collin R, Dugas V, Pelletier AN, Chabot-Roy G, Lesage S. The mouse *idd2* locus is linked to the proportion of immunoregulatory double-negative T cells, a trait associated with autoimmune diabetes resistance. *J Immunol*. 2014;193:3503–12.
- Duncan B, Nazarov-Stoica C, Surls J, Kehl M, Bona C, Casares S, et al. Double negative (CD3+ 4- 8-) TCR alphabeta splenic cells from young NOD mice provide long-lasting protection against type 1 diabetes. *PLoS One*. 2010;5:e11427.
- Crispin JC, Oukka M, Bayliss G, Cohen RA, Van Beek CA, Stillman IE, et al. Expanded double negative T cells in patients with systemic lupus

- erythematosus produce IL-17 and infiltrate the kidneys. *J Immunol.* 2008;181:8761–6.
22. Alunno A, Carubbi F, Bartoloni E, Bistoni O, Caterbi S, Cipriani P, et al. Unmasking the pathogenic role of IL-17 axis in primary Sjögren's syndrome: a new era for therapeutic targeting? *Autoimmun Rev.* 2014;13:1167–73.
 23. Alunno A, Bistoni O, Bartoloni E, Caterbi S, Bigerna B, Tabarrini A, et al. IL-17-producing CD4⁺CD8⁻ T cells are expanded in the peripheral blood, infiltrate salivary glands and are resistant to corticosteroids in patients with primary Sjögren's syndrome. *Ann Rheum Dis.* 2013;72:286–92.
 24. Alunno A, Carubbi F, Bistoni O, Caterbi S, Bartoloni E, Bigerna B, et al. CD4(-)CD8(-) T-cells in primary Sjögren's syndrome: association with the extent of glandular involvement. *J Autoimmun.* 2014;51:38–43.
 25. Zhao X, Sun G, Sun X, Tian D, Liu K, Liu T, et al. A novel differentiation pathway from CD4⁺ T cells to CD4⁺ T cells for maintaining immune system homeostasis. *Cell Death Dis.* 2016;7:e2193.
 26. Li W, Tian Y, Li Z, Gao J, Shi W, Zhu J, et al. Ex vivo converted double negative T cells suppress activated B cells. *Int Immunopharmacol.* 2014;20:164–9.
 27. Fuchs CD, Trauner M. Role of bile acids and their receptors in gastrointestinal and hepatic pathophysiology. *Nat Rev Gastroenterol Hepatol.* 2022;19:432–50.
 28. Brevini T, Maes M, Webb G J, John B V, Fuchs C D, Buescher G, et al. FXR inhibition may protect from SARS-CoV-2 infection by reducing ACE2. *Nature.* 2023;615:134–42.
 29. Erichsen TJ, Aehlen A, Ehmer U, Kalthoff S, Manns MP, Strassburg CP. Regulation of the human bile acid UDP-glucuronosyltransferase 1A3 by the farnesoid X receptor and bile acids. *J Hepatol.* 2010;52:570–8.
 30. Song P, Rockwell CE, Cui JY, Klaassen CD. Individual bile acids have differential effects on bile acid signaling in mice. *Toxicol Appl Pharmacol.* 2015;283:57–64.
 31. Campana G, Pasini P, Roda A, Spampinato S. Regulation of ileal bile acid-binding protein expression in Caco-2 cells by ursodeoxycholic acid: role of the farnesoid X receptor. *Biochem Pharmacol.* 2005;69:1755–63.
 32. Wang K, Liao M, Zhou N, Bao L, Ma K, Zheng Z, et al. Parabacteroides distasonis alleviates obesity and metabolic dysfunctions via production of succinate and secondary bile acids. *Cell Rep.* 2019;26:222–235 e225.
 33. Marchianò S, Biagioli M, Roselli R, Zampella A, Di Giorgio C, Bordoni M, et al. Beneficial effects of UDCA and norUDCA in a rodent model of steatosis are linked to modulation of GPBAR1/FXR signaling. *Biochim Biophys Acta Mol Cell Biol Lipids.* 2022;1867:159218.
 34. Winston JA, Rivera AJ, Cai J, Thanissery R, Montgomery SA, Patterson AD, et al. Ursodeoxycholic Acid (UDCA) mitigates the host inflammatory response during clostridioides difficile infection by altering gut bile acids. *Infect Immun.* 2020;88:e00045–20.
 35. Crispe IN. The liver as a lymphoid organ. *Annu Rev Immunol.* 2009;27:147–63.
 36. Willart MA, van Nimwegen M, Grefhorst A, Hammad H, Moons L, Hoogsteden HC, et al. Ursodeoxycholic acid suppresses eosinophilic airway inflammation by inhibiting the function of dendritic cells through the nuclear farnesoid X receptor. *Allergy.* 2012;67:1501–10.
 37. Miyaguchi S, Mori M. Ursodeoxycholic acid (UDCA) suppresses liver interleukin 2 mRNA in the cholangitis model. *Hepatogastroenterology.* 2005;52:596–602.
 38. Ding L, Yang L, Wang Z, Huang W. Bile acid nuclear receptor FXR and digestive system diseases. *Acta Pharm Sin B.* 2015;5:135–44.
 39. Ho PP, Steinman L. Obeticholic acid, a synthetic bile acid agonist of the farnesoid X receptor, attenuates experimental autoimmune encephalomyelitis. *Proc Natl Acad Sci U S A.* 2016;113:1600–5.
 40. Fiorucci S, Baldoni M, Ricci P, Zampella A, Distrutti E, Biagioli M. Bile acid-activated receptors and the regulation of macrophages function in metabolic disorders. *Curr Opin Pharmacol.* 2020;53:45–54.
 41. Francis M, Guo G, Kong B, Abramova EV, Cervelli JA, Gow AJ, et al. Regulation of lung macrophage activation and oxidative stress following ozone exposure by farnesoid X receptor. *Toxicol Sci.* 2020;177:441–53.
 42. Zhang H, Liu Y, Bian Z, Huang S, Han X, You Z, et al. The critical role of myeloid-derived suppressor cells and FXR activation in immune-mediated liver injury. *J Autoimmun.* 2014;53:55–66.
 43. Esmon CT. Structure and functions of the endothelial cell protein C receptor. *Crit Care Med.* 2004;32:S298–301.
 44. Kondreddy V, Wang J, Keshava S, Esmon CT, Rao LVM, Pendurthi UR. Factor VIIa induces anti-inflammatory signaling via EPCR and PAR1. *Blood.* 2018;131:2379–92.
 45. Healy LD, Fernandez JA, Mosnier LO, Griffin JH. Activated protein C and PAR1-derived and PAR3-derived peptides are anti-inflammatory by suppressing macrophage NLRP3 inflammasomes. *J Thromb Haemost.* 2021;19:269–80.
 46. Zhang ZX, Lian D, Huang X, Wang S, Sun H, Liu W, et al. Adoptive transfer of DNT cells induces long-term cardiac allograft survival and augments recipient CD4(+)Foxp3(+) Treg cell accumulation. *Transpl Immunol.* 2011;24:119–26.
 47. Tian D, Pan Y, Zhao Y, Wang H, Tian Y, Yang L, et al. TCRαβ(+)NK1.1(-) CD4(-)CD8(-) double-negative T cells inhibit central and peripheral inflammation and ameliorate ischemic stroke in mice. *Theranostics.* 2023;13:896–909.
 48. Bae HR, Leung PS, Tsuneyama K, Valencia JC, Hodge DL, Kim S, et al. Chronic expression of interferon-gamma leads to murine autoimmune cholangitis with a female predominance. *Hepatology.* 2016;64:1189–201.
 49. Terziroli Beretta-Piccoli B, Mieli-Vergani G, Vergani D, Vierling JM, Adams D, Alpini G, et al. The challenges of primary biliary cholangitis: What is new and what needs to be done. *J Autoimmun.* 2019;105:102328.
 50. Bae HR, Choi MS, Kim S, Young HA, Gershwin ME, Jeon SM, et al. IFNγ is a Key Link between Obesity and Th1-Mediated Autoimmune Diseases. *Int J Mol Sci.* 2020;22:208.

Publisher's Note

Springer Nature remains neutral with regard to jurisdictional claims in published maps and institutional affiliations.